From effective-index model to phase-plate model

Exter, M.P.; Hissink, E.S.; Koks, C.

PAPER • OPEN ACCESS

From effective-index model to phase-plate model

To cite this article: M P van Exter *et al* 2022 *J. Opt.* **24** 084001

View the article online for updates and enhancements.

From effective-index model to phase-plate model

M P van Exter ⬤, E S Hissink and C Koks

Huygens-Kamerlingh Onnes Laboratory, Leiden University, PO Box 9504, 2300 RA Leiden,
The Netherlands

E-mail: exter@physics.leidenuniv.nl

CrossMark

Abstract
In 1995, Hadley formulated an elegant effective-index model to describe the formation of transverse modes in optical cavities (Hadley 1995 *Opt. Lett.* **20** 1483–5). We apply this model to Fabry–Perot cavities and discuss its limitations, using the well-known paraxial solutions of these cavities as reference. We also introduce a new model, which we call the phase-plate model, that has less limitations and yields the correct first-order correction to the resonance frequencies for longer cavities. The analysis uses scalar optical fields in the paraxial limit.

Keywords: optical cavity, effective index, Fabry–Perot, phase plate

1. Introduction

The formation of eigenmodes in optical cavities is governed by a balance between two processes: (a) defocusing due to diffraction upon propagation, and (b) focusing due to reflection from curved mirrors or index guiding in non-uniform media. Mode formation has been studied in translation invariant structure like optical waveguides and fibers [1, 2]. But also in optical cavities, like open Fabry–Perot (FP) cavities [3] and the monolithic cavities used for microlasers [4] and vertical-cavity surface-emitting lasers (VCSELS) [5, 6]. Open micro cavities [7] and monolithic cavities are, among others, of interest for quantum communication [8, 9].

The effective-index model is an elegant and powerful method to describe mode formation in optical cavities. The simplest version of this model, derived in this paper, assumes that the effects of diffraction and index guiding can be spread uniformly over the optical cavity length. Mode formation in such a cavity resembles mode formation in an optical fiber [2]. This model, however, only works for short cavities.

In this paper, we apply the effective-index model to a two-mirror FP cavity and address the question when and how this model breaks down for longer cavities. We also introduce an alternative model, the so-called phase-plate model, which also works for longer cavities. Both models use a scalar paraxial approximation of the optical field. This approximation is valid when typical beam widths are much larger than the optical wavelength and typical angles are small (paraxial). More extended, vector non-paraxial, descriptions of the field are needed for the general case [10–16].

Figure 1 shows the three cavity geometries that we compare in this paper. The left figure shows a plano-concave FP cavity, with a planar mirror and a concave mirror with radius R positioned at a distance L. The middle figure shows the simple effective-index model of this cavity, where the concave mirror is replaced by a flat mirror and the uniform medium is replaced by a (fictitious) medium with a position-dependent effective index $n_{eff}(x, y)$. The right figure shows the phase-plate model of this cavity, where the concave mirror is replaced by a phase plate on a flat mirror and the medium remains uniform. Section 2 describes the transition from the FP cavity to the effective-index model. Section 3 compares the paraxial solutions of the FP cavity with the solutions of the effective-index model to show that they agree only in the short-cavity limit. Section 4 introduces a new phase-plate model to demonstrate that this model also works for longer cavities.
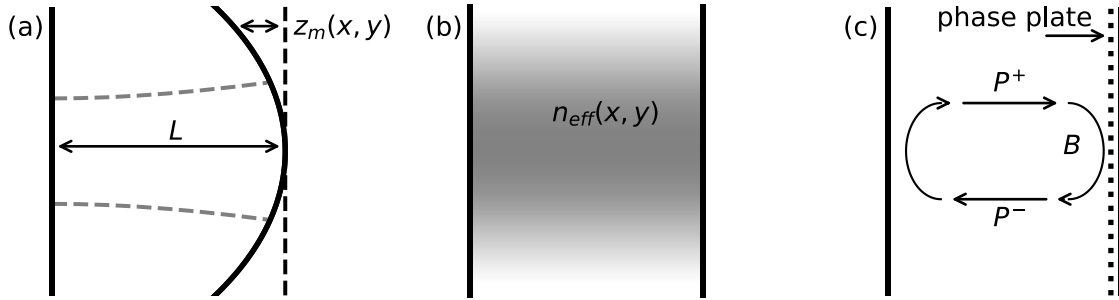
Figure 1. Three geometries for FP cavities with equal cavity length L and equal guiding from three different mechanisms: (a) modes in a plano-concave cavity depend on the mirror shape $z_m(x,y)$, (b) modes in an effective-index cavity depend on the index profile $n_{eff}(x,y)$, (c) modes in a phase-plate cavity depend on the phase profile acquired upon reflection from the phase-plate mirror. Figure (c) shows how the cavity roundtrip operator $M = P^- B P^+$ combines forward propagation P^+, reflection B, and backward propagation P^-.

2. Effective-index model applied to FP cavities

The effective-index model [4–6, 17] is based on a mathematical trick to partially separate the longitudinal and transverse variations of the field in an optical cavity. It does so by writing the intra-cavity field as $E(x,y,z) = f(x,y;z)\Phi(x,y)$, where $f(x,y;z)$ is the resonant intra-cavity field expected for a planar cavity with a longitudinal structure equal to the structure of the real cavity at transverse position (x,y). The (x,y) dependence of the associated resonances translates into an effective-index $n_{eff}(x,y)$ that determines the formation of the transverse eigenmodes $\Phi(x,y)$ in the real cavity.

The full effective-index model of Hadley [17] includes the standing wave character and curvature of the field. This is relevant for complicated cavities like VCSELs [5, 6], where the placement of intra-cavity elements in nodes or anti-nodes of the field have different effects, but not for open/empty FP cavities. Similarly, the difference between group and phase index is relevant for VCSELs [5] but not for air-based cavities. FP cavities can hence be described with a simpler, more intuitive, version of the effective-index model, which we will derived from the wave equation.

When we apply the effective-index model to a plano-concave FP cavity, the planar-cavity modes are standing waves of the form $f(x,y;z) = f_0 \sin[k_z(x,y)z]$, with $k_z(x,y)L(x,y) = q\pi$ and integer (longitudinal mode number) q to satisfy the boundary conditions at the two mirrors. The on-axis cavity length $L = L(0,0)$ defines the reference wave vector $k_0 = q\pi/L$. The position-dependent cavity length $L(x,y) = L - z_m(x,y)$, with mirror shape $z_m(x,y)$, defines an effective-index profile $n_{eff}(x,y) = L(x,y)/L$. Together this yields $k_z(x,y) = k_0/n_{eff}(x,y)$.

Next, we substitute $E(x,y,z) = f(x,y;z)\Phi(x,y)$ with the described form of $f(x,y;z)$ in the wave equation $(\partial^2/\partial z^2 + \Delta_\perp + k^2)E = 0$, with $\Delta_\perp = \partial^2/\partial x^2 + \partial^2/\partial y^2$. This yields the effective-index equation

$$\left(\Delta_\perp + k^2 - \frac{k_0^2}{n_{eff}^2(x,y)}\right)\Phi(x,y) = 0, \qquad (1)$$

if one neglects the transverse derivatives of $f(x,y;z)$, i.e. if one neglects $\Phi\Delta_\perp f$ and $2\vec{\nabla}_\perp f \cdot \vec{\nabla}_\perp \Phi$ with respect of $f\Delta_\perp\Phi$. The

eigenvalues $k = k_j$ of equation (1) describe the resonance frequencies $\omega_j = k_j c$ of the optical cavity. Its solutions $\Phi_j(x,y)$ describe the associated transverse eigenmodes.

For the typical case $1 - n_{eff} = z_m/L \ll 1$ we simplify equation (1) by writing $k = k_j = k_0 + \delta k_j$ and expanding k^2 and n_{eff}^2, to obtain the dimensionless form

$$\left(-\frac{\Delta_\perp}{2k_0^2} + \frac{z_m(x,y)}{L}\right)\Phi_j(x,y) \approx \frac{\delta k_j}{k_0}\Phi_j(x,y). \qquad (2)$$

This equation resembles the eigenvalue equation of a quantum mechanical wavefunction $\Phi(x,y)$ and shows how the mirror profile acts as an effective potential for the transverse mode profile. For the typical case $z_m \geqslant 0$, the resonance frequencies of the guides modes are (somewhat) larger than those of the planar cavity ($\delta k_j > 0$), to compensate for the phase lag acquired upon propagation and for the shorter effective cavity length of the concave cavity ($n_{eff} \leqslant 1$).

Finally, we consider a plano-concave cavity with a paraboloidal mirror shape $z_m(x,y) \approx r^2/2R$ with paraxial radius of curvature R. This 2D rotational symmetric geometry supports several families of transverse modes [18–21], like Hermite–Gaussian, Laguerre–Gaussian, and Ince–Gaussian modes, including elegant/complex versions thereof, which share a common fundamental mode size γ, with $\gamma^2 = \sqrt{LR}/k$. Members of one family can be transformed into members of another family due to the frequency degeneracy within these families [22]. We will focus on the family of Hermite–Gaussian modes, because their 2D mode profiles factorize as $HG_{n_x}(x) \times HG_{n_y}(y)$, such that a 1D analysis suffices. The relative resonance frequencies of these modes are

$$\frac{\delta k_j}{k_0} = \frac{1}{(k\gamma)^2}(1 + n_x + n_y) = \frac{1}{k\sqrt{LR}}(1 + n_x + n_y), \qquad (3)$$

with integer transverse modes numbers n_x and n_y.

3. Paraxial solutions for FP cavities

In this section, we compare the effective-index results with the well-known paraxial solutions for plano-concave cavities. We present these solutions by writing the forward-propagating optical field in its scalar slowly-varying form

$E(x,y,z) = \psi(x,y,z)\exp(ikz)$, where $\psi(x,y,z)$ satisfies the paraxial wave equation $[2ik(\partial/\partial z) + \Delta_\perp]\psi = 0$. We again focus on the Hermite–Gaussian solutions, which factorize as $\psi_{n_x,n_y}(x,y,z) = \psi_{n_x}(x,z)\psi_{n_y}(y,z)$, where

$$\psi_{n_x}(x,z) = \frac{C}{\sqrt{\gamma(z)}} H_{n_x}\left(\frac{x}{\gamma(z)}\right)\exp\left[-\frac{x^2}{2\gamma^2(z)} + i\phi(x,z)\right],$$

$$\phi(x,z) = \frac{kx^2}{2R(z)} - \left(n_x + \frac{1}{2}\right)\chi_0(z), \qquad (4)$$

with normalization constant C, and likewise for $\psi_{n_y}(y,z)$. The paraxial solution contains three important functions of z: (a) the beam width $\gamma(z)$, (b) the radius of wave-front curvature $R(z)$, and (c) the phase lag $\chi_0(z)$ of the fundamental beam with respect to a plane wave. The beam width $\gamma(z) = \gamma_0\sqrt{1 + z^2/z_0^2}$, with Rayleigh range $z_0 = \sqrt{L(R-L)}$ and beam waists $\gamma_0 = (z_0/k)^{1/2}$ and $\gamma_1 = \sqrt{R/(R-L)}\gamma_0$ at the planar and curved mirror, respectively. The radius of curvature $R(z) = z + z_0^2/z$. The fundamental phase lag $\chi_0(z) = \arctan(z/z_0)$ yields the (single-pass) Gouy phase $\chi_0(L) = \arcsin\sqrt{L/R}$ for $z = L$. The phase lag is $\chi_0(z)$ for the fundamental 2D mode and a factor $(n_x + n_y + 1)$ larger for higher-order 2D modes.

How do the predictions of the effective-index model compare with the exact paraxial result for these three parameters $\gamma(z)$, $R(z)$ and $\chi_0(z)$? First, the typical mode size $\gamma = (LR/k^2)^{1/4}$ in the effective-index model is the geometric mean between the paraxial beam size at both mirrors, i.e. $\gamma = \sqrt{\gamma_0\gamma_1}$. This is a reasonable result for a model that averages over the cavity length. Second, the wave-front curvature of the intra-cavity field $E(x,y,z) = f(x,y;z)\Phi(x,y)$, included in $f(x,y;z)$, varies linearly with position, i.e. $1/R(z) \approx (z/L)/R$, in the full effective-index model. This resembles the paraxial result $[1/R(z)] = z/(z_0^2 + z^2) = z/(LR + z^2 - L^2)$, but only when $L/R \ll 1$.

Third and most important, we compare the effective-index result of equation (3), with the paraxial result for the associated phase lag per unit length

$$\begin{aligned}\frac{\delta k_j}{k} &= \frac{\chi_{n_x,n_y}(L)}{kL} = \frac{1 + n_x + n_y}{kL}\arcsin\sqrt{\frac{L}{R}} \\ &\approx \frac{1 + n_x + n_y}{k\sqrt{LR}}\left(1 + \frac{L}{6R}\right).\end{aligned} \qquad (5)$$

This comparison shows that the effective-index result approaches the exact paraxial result only for short ($L \ll R$) cavities, but misses a factor $(1 + L/6R)$ for longer cavities. The next section shows how this factor is recovered in the phase-plate model.

4. Phase-plate model and roundtrip operator

The phase-plate model replaces the concave mirror of a plano-concave FP cavity by a flat mirror covered with a fictitious phase plate that adds a phase factor $\exp[-i2kz_m(r)]$, with $z_m = $

$r^2/2R$, to the reflection. This phase factor makes the reflection from the planar mirror plus phase plate in figure 1(c) similar to the reflection from the curved mirror in figure 1(a). But not identical, as light propagates slightly less (typically $<\lambda$) in the real cavity than in the phase-plate model cavity. Still, we expect the phase-plate model to give a more realistic description of the actual physics than the effective-index model, because it keeps the reflection phase located at the mirror and does not spread it over the full cavity length.

We analyze the resonances of the phase-plate cavity with the roundtrip formalism, which describes the change of the complex field amplitude $\psi(x,y;z)$ per roundtrip as $\psi \to M\psi$ with the roundtrip operator M [23–25]. Starting from the plane mirror, the roundtrip operator $M_{-+} = P^- BP^+$, where P^+ and P^- represent the forward and backward propagation between the two mirrors and B represents the reflections from the curved mirror (see figure 1(c)). We split this reflection in two halves, via $B = \tilde{B}^2$, and note that the propagators are equal after unfolding of the cavity, making $P^+ = P^- = P(L) = \tilde{P}$. With these definitions, we have

$$M_{-+} = \tilde{P}\tilde{B} \times \tilde{B}\tilde{P} \equiv \exp(iZ_-) \times \exp(iZ_+), \qquad (6)$$

where $\exp(iZ_+)$ describes the forward path and $\exp(iZ_-)$ the backward path. If we would have started the roundtrip at a fictitious point halfway between the reflection from the curved mirror, the roundtrip operator would be $M_{+-} = \tilde{B}\tilde{P} \times \tilde{P}\tilde{B} = \exp(iZ_+) \times \exp(iZ_-)$. We expect that these two roundtrip operators have identical eigenvalues, as they describe the same physics, but eigenmodes that differ by an operator factor $\exp(iZ_\pm)$, as they are mathematically related via a unitary transformation.

The propagation and reflection operators are

$$\tilde{P} = \exp\left[i\frac{L}{2k}\left(\frac{\partial^2}{\partial x^2} + \frac{\partial^2}{\partial y^2}\right)\right], \qquad (7)$$

$$\tilde{B} = \exp\left[-i\frac{k}{2R}(x^2 + y^2)\right]. \qquad (8)$$

Equation (7) follows from the paraxial wave equation with the general propagator $P(z)$, defined via $\psi(x,y;z+\Delta z) = P(\Delta z)\psi(x,y;z) \Rightarrow dP(z)/dz = (i/2k)\Delta_\perp P(z)$. It also follows from the $\exp(ik_z z)$ evolution of EM plane waves with the Taylor expansion of the on-axis momentum $k_z = \sqrt{k^2 - k_\perp^2} \approx k - k_\perp^2/(2k)$, with $k_\perp^2 = -(\partial^2/\partial x^2 + \partial^2/\partial y^2)$. Equation (8) describes half the phase acquired upon reflection from the curved mirror.

The solutions of the phase-plate model tend to differ from those of the effective-index model because the operators $\tilde{P}$ and $\tilde{B}$ do not commute. But the phase-plate model does reduce to the effective-index model when the effects of propagation and reflection are spread uniformly over the cavity, i.e. if we modify

$$\tilde{P}\tilde{B} \to \lim_{N\to\infty} (\tilde{P}^{1/N}\tilde{B}^{1/N})^N, \qquad (9)$$

and likewise for $\tilde{B}\tilde{P}$. This division is equivalent to writing the evolution of the field as

$$\frac{\partial}{\partial z}\psi = \left[\frac{i}{2k}\left(\frac{\partial^2}{\partial x^2} + \frac{\partial^2}{\partial y^2}\right) - \frac{ik}{2LR}(x^2 + y^2)\right]\psi, \quad (10)$$

because $\Delta z = L/N \rightarrow \delta z$ (infinitesimal line element) in the limit $N \rightarrow \infty$. Equation (10) is identical to the effective-index equation (2) for a cavity with a spherical mirror, where $\partial\psi_j/\partial z = -i\delta k_j\psi_j$ is the spread-out phase lag. It is also equivalent to the Schrödinger equation for the 2D harmonic oscillator, where z acts as time coordinate for the corresponding quantum oscillator [26].

Even though $\tilde{P}$ and $\tilde{B}$ do not commute, one can still determine the eigenvalues and eigenmodes of certain combinations of these operators. We will perform this analysis for one transverse direction (x only); the result is the same for the y direction and the two results can be simply combined afterwards. To further simplify the equations, we introduce dimensionless coordinates $\xi_x = x/\gamma$ and $\xi_y = y/\gamma$, with $\gamma^2 = \sqrt{LR}/k$, and write the x-part of the operators as

$$\tilde{P}_x = \exp(iX) \text{ with } X = \frac{1}{2}\sqrt{\frac{L}{R}}\frac{\partial^2}{\partial\xi_x^2}, \quad (11)$$

$$\tilde{B}_x = \exp(iY) \text{ with } Y = -\frac{1}{2}\sqrt{\frac{L}{R}}\xi_x^2. \quad (12)$$

The Baker–Campbell–Hausdorff (BCH) relation allows one to express the product of two unitary operators as a single unitary operator, to more easily find its eigenvalues and eigenmodes. We first apply this relation to the (x components of the) combined operators $\exp(iZ_+) = \exp(iY) \cdot \exp(iX)$ and $\exp(iZ_-) = \exp(iX) \cdot \exp(iY)$ to find

$$iZ_\pm = i(X+Y) \pm \frac{1}{2}[X,Y] + \frac{i}{12}([Y,[X,Y]] - [X,[X,Y]) + \cdots \quad (13)$$

where $[X,Y] = XY - YX$ is the commutator. The consecutive terms in this equation obey the commutation relations

$$[X,Y] = -\frac{L}{R}\left(\frac{1}{2} + \xi\frac{\partial}{\partial\xi}\right), \quad (14)$$

$$[X,[X,Y]] = -\left(\frac{L}{R}\right)^{1.5}\frac{\partial^2}{\partial\xi^2} = -\frac{2L}{R}X, \quad (15)$$

$$[Y,[X,Y]] = -\left(\frac{L}{R}\right)^{1.5}\xi^2 = \frac{2L}{R}Y. \quad (16)$$

These equations show that the relative strengths of the higher-order terms in the expansion of $iZ_\pm$ scale with powers of $\sqrt{L/R}$. Furthermore, the simple form of the double commutators results in a recursion relation between the higher-order terms in the BCH expansion and in the generic equation

$$iZ_\pm = if\left(\frac{L}{R}\right)(X+Y) \pm \frac{L}{2R}g\left(\frac{L}{R}\right)\left(\frac{1}{2} + \xi\frac{\partial}{\partial\xi}\right), \quad (17)$$

with functions $f(L/R) = 1 + L/(6R) + \mathcal{O}(L^2/R^2)$ and $g(L/R) = 1 + L/(6R) + \mathcal{O}(L^2/R^2)$, where $\mathcal{O}$ indicates the next order in each Taylor expansion.

Finally, we combine the two single-path operators into a roundtrip operator, using either $M_{-+} = \exp(iZ_-)\exp(iZ_+)$ or its companion $M_{+-} = \exp(iZ_+)\exp(iZ_-)$. We already noted that the eigenvalues of M_{+-} and M_{-+} should be identical, although their eigenvectors will typically differ by a factor $\exp(iZ_\pm)$. Hence, we only consider eigenvalues of the sum operator $i(Z_+ + Z_-)$. Using the operators and commutators given above, and the first-order Taylor expansion of $f(L/R)$, we find

$$i(Z_+ + Z_-)|\psi_{n_x,n_y}\rangle \approx -2i\sqrt{\frac{L}{R}}\left(1 + \frac{L}{6R}\right)(1 + n_x + n_y)|\psi_{n_x,n_y}\rangle, \quad (18)$$

for the roundtrip phase lag. This result is consistent with the first-order Taylor expansion of the (single-pass) paraxial phase lag $\chi_0(L) = \arcsin\sqrt{L/R} \approx \sqrt{L/R}[1 + L/(6R)]$, presented in equation (5). It presents the promised first-order correction to the (incorrect) resonance frequencies of consecutive transverse modes as derived from the effective-index model.

We end with the remark that the analysis presented in this paper uses paraxial scalar fields. One might wonder which corrections would appear for non-paraxial vector fields. This calculation is complicated [10–16], but the bottom line is that non-paraxial and vector effects on $\delta k_j/k$ are order $1/(k^2LR)$. Hence, it is typically not necessary to go beyond the paraxial phase-plate model, which predicts a typically larger correction of the order $\sqrt{L/R}/(kR)$ with respect to the effective-index model. Non-paraxial vector corrections are important though when one is interested in the fine structure in the resonance spectrum of the transverse modes [24, 25].

5. Concluding summary

This paper applied the effective-index model to plano-concave FP cavities and analyzed the resulting predictions for the resonance frequencies and eigenmodes. The resulting effective-index equation was shown to be identical to the eigen-value problem of a quantum-mechanical wavefunction, where the effective-index profile $n_{\text{eff}}(x,y)$ acts as a 2D potential. The paper discussed the limitations of the effective-index model, showed that the model works fine for very short cavities ($L \ll R$), and introduced corrections of the order $L/6R$ for slightly longer cavities. Finally, it introduced the phase-plate model as an alternative model that also works for slightly longer cavities and showed that this model correctly describes the mentioned first-order correction. Non-paraxial effects are not included and are expected to be smaller than the mentioned paraxial correction.

Data availability statement

No new data were created or analysed in this study.

ORCID iD

M P van Exter ⓘ https://orcid.org/0000-0003-0839-3219

References

[1] Saleh B E A and Teich M C 2007 *Fundamentals of Photonics* (New York: Wiley)
[2] Snyder A W and Love J D 1983 *Optical Waveguide Theory* (Berlin: Springer)
[3] Siegman A E 1988 *Lasers* (Mill Valley, CA: University Science Books)
[4] Serrat C, van Exter M P, van Druten N J and Woerdman J P 1999 Transverse mode formation in microlasers by combined gain- and index-guiding *IEEE J. Quantum Electron.* **35** 1314–21
[5] Wenzel H and Wunsche H J 1997 The effective frequency method in the analysis of vertical-cavity surface-emitting lasers *IEEE J. Quantum Electron.* **33** 1156–62
[6] Hegblom E R, Babic D I, Thibeault B J and Coldren L A 1997 Scattering losses from dielectric apertures in vertical-cavity lasers *IEEE J. Sel. Top. Quantum Electron.* **3** 379–89
[7] Trichet A A P, Dolan P R, Coles D M, Hughes G M and Smith J M 2015 Topographic control of open-access microcavities at the nanometer scale *Opt. Express* **23** 17205
[8] Somaschi N *et al* 2016 Near-optimal single-photon sources in the solid state *Nat. Photon.* **10** 340–5
[9] Najer D *et al* 2019 A gated quantum dot strongly coupled to an optical microcavity *Nature* **575** 622
[10] Lax M 1975 From Maxwell to paraxial wave optics *Phys. Rev.* A **11** 1365–70
[11] Yu P K and Luk K M 1983 High-order azimuthal modes in the open resonator *Electron. Lett.* **19** 539–41
[12] Luk K M 1986 Improvement in the resonant formula of a spherical Fabry–Perot resonator with unequal mirrors *J. Opt. Soc. Am.* A **3** 3

[13] Nasalski W 2006 Polarization versus spatial characteristics of optical beams at a planar isotropic interface *Phys. Rev.* E **74** 056613
[14] Nasalski W 2018 Elegant Laguerre–Gaussian beams—formulation of exact vector solution *J. Opt.* **20** 105601
[15] Aiello A 2020 Field theory of monochromatic optical beams: I. Classical fields *J. Opt.* **22** 014001
[16] Aiello A 2020 Field theory of monochromatic optical beams: II. Classical and quantum paraxial fields *J. Opt.* **22** 014002
[17] Hadley G R 1995 Effective-index model for vertical-cavity surface-emitting lasers *Opt. Lett.* **20** 1483–5
[18] Bandres M A and Gutiérrez-Vega J C 2004 Ince–Gaussian beams *Opt. Lett.* **29** 144–6
[19] Bandres M A 2004 Elegant Ince–Gaussian beams *Opt. Lett.* **29** 1724–6
[20] Elahi P, Nadgaran H and Fard F K 2005 Longitudinally modes characteristics of Ince–Gaussian beams in laser resonators with quadratic-index active medium *Proc. CAOL 2005. 2nd Int. Conf. on Advanced Optoelectronics and Lasers* vol 1 pp 218–21
[21] Alpmann C, Schoeler C and Denz C 2015 Elegant Gaussian beams for enhanced optical manipulation *Appl. Phys. Lett.* **106** 241102
[22] Kimel I and Elias L R 1993 Relations between Hermite and Laguerre Gaussian modes *IEEE J. Quantum Electron.* **29** 2562–7
[23] Kleckner D, Irvine W T M, Oemrawsingh S S R and Bouwmeester D 2010 Diffraction-limited high-finesse optical cavities *Phys. Rev.* A **81** 043814
[24] van Exter M P, Wubs M, Hissink E S and Koks C 2022 Fabry–Perot microcavity spectra have a fine structure (arXiv:2203.01638)
[25] Koks C, Baalbergen F B and van Exter M P 2022 Observation of microcavity fine structure (arXiv:2203.01200)
[26] Nienhuis G 2021 Operators in paraxial quantum optics *Structured Light for Optical Communication* ed M D Al-Amri, D L Andrews and M Babiker (Amsterdam: Elsevier) ch 5